Kathford Journal of Engineering and Management,
ISSN: 2661-6106.

https://kathford.edu.np/Journal/

VOL. 3 ISSUE 1 JUNE 2023, pp. 149-171

BLADE STRUCTURE ANALYSIS OF 2 MW V-SHAPED VERTICAL AXIS WIND TURBINE USING NUMERICAL SIMULATION

Aastik Sharma[1,2], Lei Zhang[1], Jianjun Qu[1,*], Sagar Panthi[3], Janak Kumar Tharu[4]
[1]School of Mechatronic Engineering, Harbin Institute of Technology, Harbin, China, [2]Department of Civil Engineering, Kathford International College of Engineering & Management, Lalitpur, Nepal,[3]Department of Mechanical Engineering, Beijing Institute of Technology of Technology, Beijing, China, [4]Department of Civil Engineering, Nepal Engineering College

[*]Corresponding author: *qujianjun@hit.edu.cn*

ABSTRACT – The intensive research on large-scale Vertical Axis Wind Turbine (VAWT) could provide an alternative to Horizontal Axis Wind Turbine (HAWT) in offshore deployment for the future. Regarding this fact, this article develops a conceptual design of the VAWT blade structure and analyzes its feasibility using numerical simulation. The blade structure is designed for 2 MW Darrieus type V- shaped VAWT. The blade is tapered, 90m long, and inclined at 35° to the vertical axis. Initially, the blade design is tested for ultimate strength test according to IEC 61400-01 standard using aluminum alloy and homogenized composite material. In doing so, maximum aerodynamic loading on the blade is calculated after steady state 3-D RANS CFD simulation of the blade in ANSYS Fluent. The Finite Element Method (FEM) model of the blade is created using shell element in ANSYS Static Structural with structured meshing strategy, and tested with the aerodynamic load using the one-way Fluid-Structure Interaction (FSI) technique, to obtain mesh independent solution. The impact of the using 2, 3, and 4 number of shear webs is then analyzed on the selected mesh model of the blade. Finally, a four-shear web model of the blade is tested under extreme conditions. The thickness of the blade surface and shear web are varied to test maximum deflection at the tip, and maximum allowable strain of the blade. After obtaining the required blade structure, the deformation, maximum equivalent stress, and maximum equivalent strain for the blade are studied at rotation Tip Speed Ratio (TSR) of 5 under aerodynamic and gravitational loading, using both materials. The study showed significant deflection at the tip of the blade for the tower-less V-VAWT blade, suggesting an alternative support mechanism for the blade. Also, the study concluded that better structural robustness is achieved while using a composite material instead of an aluminum alloy. This article provides basis to study structural behavior of the novel V-VAWT blades and contribute to continuing research on obtaining optimized blade structure for such turbine.

KEYWORDS – ***VAWT, CFD, FEM, FSI, Blade structure***

Kathford Journal of Engineering and Management,
ISSN: 2661-6106.

https://kathford.edu.np/Journal/

VOL. 3 ISSUE 1 JUNE 2023, pp. 149-171

1. INTRODUCTION

The scope of Darrieus large-scale Vertical Axis Wind Turbine (hereafter, VAWT) for offshore applications is promising because of its simpler design and location of its heavy components like the gearbox and generator at the base of its turbine. Due to this, the installation, operation and maintenance cost of VAWT in offshore area decreases as compared to Horizontal Axis Wind Turbine (hereafter, HAWT).Moreover, the VAWT has a better stability because of lower moment of inertia and requires lighter substructure than HAWT for offshore deployment (Tjiu, Marnoto, Mat, & Ha, 2015). However, the non-conventional designs of the VAWT need intense research for optimization to be commercially viable (Tjiu, Marnoto, Mat, Ruslan, et al., 2015). Apart from the decent aerodynamic efficiency (Griffith et al., 2018), the structural ability of the VAWT requires significant consideration. Therefore, this article intends to study the structural robustness of a 2 MW V-shaped VAWT's blade under different loading conditions.

Different materials have been used to provide strength and durability for the VAWT blades. Aluminum 6063-T5, using an extrusion process, was used by SNL and other contemporary VAWT manufacturers in the 1970s, 80s, and 90s. It was later known that this material has poor fatigue properties, $5 * 10^8$ cycle, which led to early fractures in turbine blades (Sutherland et al., 2012). As the operating life of a wind turbine blade is 20-30 years, the turbine blade should be able to withstand at least 10^9 cycles, fatigue properties of the blade material provide significant impact, and hence must be considered seriously(Sutherland et al., 2012). The use of epoxy glass fiber has improved the fatigue properties of the blade in case of HAWT(Tangler, 2000). In the case of a modern-day wind turbine, it is a complex structure comprising different layers of composite material to obtain the desired properties of the blade. An example of these turbine blade structure is shown in Figure 1(b). Turbine blades consist of unidirectional, biaxial, and tri-axial composite materials having orthotropic properties(Tarfaoui et al., 2020). Most abundantly, Glass Fiber Reinforced Polymer (hereafter, GFRP) or even Carbon Fiber Reinforced Polymer (hereafter, CGRP) in some critical areas are often used in large-scale wind turbine blades(Ullah et al., 2020) to improve strength and fatigue life of the blade. The blade also consists of core material sandwiched between two unidirectional composite layers to provide more stiffness to the blade. Nexus and Gelcoat are applied on the surface of the blade to obtain a high-quality aerodynamic surface (Hand et al., 2021). These combinations of the advanced materials provide significant structural support for the wind turbine blade.

Kathford Journal of Engineering and Management,
ISSN: 2661-6106.

https://kathford.edu.np/Journal/

VOL. 3 ISSUE 1 JUNE 2023, pp. 149-171

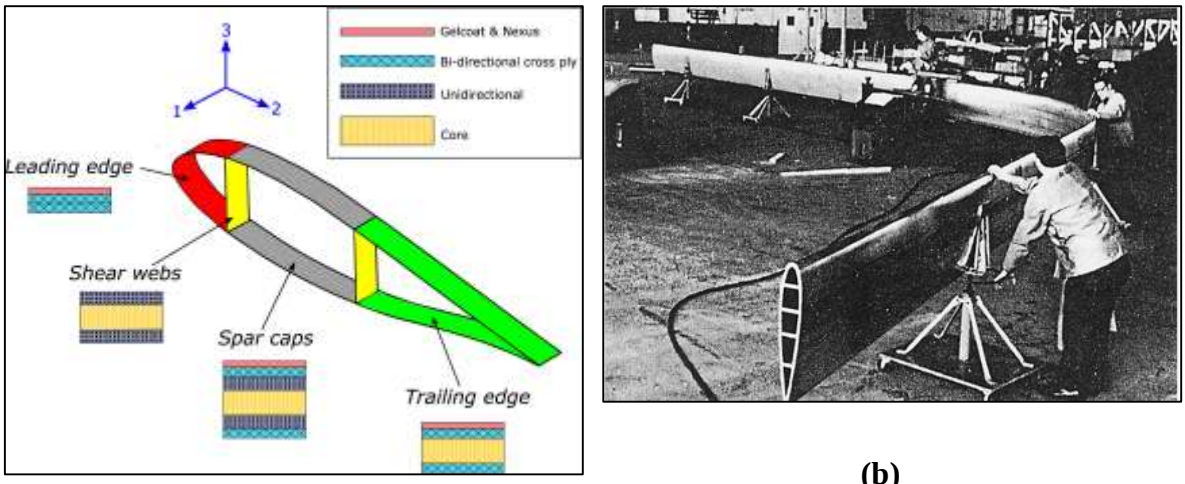

(a) **(b)**

Figure 1. (a) Blade internal structure and material schematic(Hand et al., 2021), (b) 17-m Darrieus blade by Alcoa in the 1970s (Tjiu, Marnoto, Mat, Ruslan, et al., 2015)

For VAWT, there have been several studies in recent times using composite material (Hand et al., 2021; Owens & Griffith, 2014; Wang et al., 2016). The detailed fatigue and ultimate strength analysis of the large-scale H-shaped VAWT with Finite Element Method (hereafter, FEM) modeling of the laminate layer of composite material used in a turbine blade was done by Lin et al in 2019 (Lin et al., 2019). These studies have shown that composite materials, although expensive, could provide the required structural support in the large-scale VAWT. Beside this, the structural support to VAWT is also provided by the geometry of the blade. The spar caps located at the maximum thickness resist the flapwise bending and the shear web's structure resists the torsional loads for the turbine blade(Barnes & Morozov, 2016). The number of shear webs used for VAWT also varies according to the study. The 17-m VAWT blade by Alcoa had 4 shear webs as shown in Figure 1(a). Brian, Kelly, and Cashman used 2 shear web models for their 5-MW H-shaped VAWT (Hand et al., 2021). Lin, Xu, and Xia did the structural analysis of large-scale VAWT with 5 shear web model (Lin et al., 2019). This article analyzes aluminum and homogenized composite material for the blade with varying numbers of shear webs.

This paper intends to develop a conceptual design of the blade structure for the V-VAWT blade. The V-VAWT blade is designed for a 2 MW tower-less turbine model. It is 90 m long inclined at 35 degrees to the vertical axis and tapered towards the tip, with a base chord length of 5m and tip chord length of 2m. The blade profile is made up of NACA 0012 airfoil. The concept is somehow similar to the 10 MW Aerogenerator-X (David & Julia, n.d.). Aerogenerator-X has a rotor

Kathford Journal of Engineering and Management,
ISSN: 2661-6106.

https://kathford.edu.np/Journal/

VOL. 3 ISSUE 1 JUNE 2023, pp. 149-171

diameter of 270m and height of 130m; the two inclined blades of the turbine consisted of airfoils surface mounted at the end. However, the V-shaped blade doesn't have an airfoil surface at the tip.

2. METHODOLOGY

In the course of developing the blade structure, we at first performed the ultimate strength test of the different blade structures using aluminum alloy and composite material properties under extreme loading conditions according to IEC standards (Commision, 2014). Properties of both the materials are listed in Table 1. The aerodynamic load was calculated after performing a 3D Computational fluid dynamic (hereafter, CFD) simulation of the blade. Then, using Fluid-Structure Interaction (hereafter, FSI), the deformation and maximum stress concentration of the blade were analyzed. The mesh independency test for FEM simulation was performed to improve the accuracy of the results. A blade model was selected based on the calculated thickness of the blade and the location of the shear webs. The model was then studied under aerodynamic and gravitational loading at different azimuthal positions. The study is carried out by performing the transient RANS CFD simulation for the blade at the designed Tip Speed Ratio tip speed ratio (hereafter, TSR). Subsequently, through FSI, the deformation, and maximum stress concentration of the blade at eight different azimuth positions are calculated.

Table 1: Mechanical and strength properties for (a) Aluminum alloy and (b) Homogenized composite material(Brøndsted et al., 2005)

(a)

Material properties	Value	Unit
Density	2700	kg/m^3
Young's Modulus	7.1E10	Pa
Poisson's Ratio	0.33	-
Shear Modulus	2.6629E10	Pa
Tensile yield strength	2.8E8	Pa
Tensile ultimate strength	3.1E8	Pa

(b)

Material properties	Value	Unit
Density	1550	k/m^3
Young's Modulus-X	1.1375E11	Pa
Young's Modulus-Y	7.583E9	Pa
Young's Modulus-Z	7.583E9	Pa
Poisson's Ratio-XY	0.32	-
Poisson's Ratio-YZ	0.37	-
Poisson's Ratio-XZ	0.35	-
Shear Modulus-XY	5.446E9	Pa

Kathford Journal of Engineering and Management,
ISSN: 2661-6106.

https://kathford.edu.np/Journal/

VOL. 3 ISSUE 1 JUNE 2023, pp. 149-171

	Shear Modulus-YZ	2.946E9	Pa
	Shear Modulus-XZ	2.964E9	Pa

2.1. IEC standard

The wind turbines are subjected to various operational and external conditions during their service life. International Electrotechnical Commission (IEC 61400-01)(Commision, 2014)and Germainscher Lyoyd (GL) guideline establishes safety requirements for wind turbines. The load cases and analysis type (i.e., ultimate strength and fatigue) are determined by the combination of operational and external conditions defined by the guidelines. The operational conditions of Table **2** shows an IEC standards and classes.

a wind turbine are divided into a normal, fault, after the occurrence of a fault, and erection, transportation, and maintenance. External conditions are classified into two groups as normal and extreme. For ultimate strength analysis, operational conditions don't have a significant role. From the external conditions, this study considered the extreme wind speeds. For extreme wind load, V-VAWT was classified according to IEC 61400-01 (Commision, 2014) design standard and the Class IA.

Table 2: IEC wind turbine class design (Commision, 2014)

Parameters (m/s)	Class I	Class II	Class III	Class IV
Average wind velocity	10	8.5	7.5	6
Reference wind velocity	50	42/5	37.5	30
50-year return gust wind velocity	70	59.5	52.5	42

The IEC standard defines a 50-year extreme wind condition as one of the most critical load cases where the turbine is stationary (i.e. $\omega = 0$). The IEC 61400-01 standard defines the 50-year return gust value, as 1.4 times the 50-year return 10 min wind speed of 50 m/s. That is to say, the turbine must be able to withstand a maximum wind velocity of 70 m/s.

Thus, the extreme load case is the largest flapwise bending experienced by the blade because of the maximum wind velocity that the wind turbine is expected to encounter in its lifetime. For V-VAWT, the blade experiences a cross-wind at an angle of attack of 90 degrees where the flapwise bending load will be maximum. The aerodynamic load on the

Kathford Journal of Engineering and Management,
ISSN: 2661-6106.

https://kathford.edu.np/Journal/

VOL. 3 ISSUE 1 JUNE 2023, pp. 149-171

V-VAWT blade due to 70 m/s of wind needs to be calculated.

2.1.1 Study of the blade thickness for ultimate strength loading condition

On the application of the load, the tensile (Eq. 1) and compressive (Eq. 2) strains developed on the blade must not exceed the material allowable strains.

$$\epsilon_{t,max} \leq \epsilon_{t,allow} \quad (1)$$

$$\epsilon_{c,max} \leq \epsilon_{c,allow} \quad (2)$$

Where $\epsilon_{t,allow}$ and $\epsilon_{c,allow}$ are allowable

$$\epsilon_{t,allow} = \frac{\epsilon_{t,ulti}}{f_s} \quad (3)$$

$$\epsilon_{c,allow} = \frac{\epsilon_{c,ulti}}{f_s} \quad (4)$$

tensile and compressive strain

Where $\epsilon_{t,ulti}$ and $\epsilon_{c,ulti}$ are ultimate tensile (Eq. 3) and compressive (Eq. 4) strains, respectively. For aluminum alloy, both the tensile and compressive ultimate strains are calculated as:

$$\epsilon_{ulti} = \frac{Tensile\ ultimate\ strength}{Young's\ modulus} = \frac{3.1 * 10^8}{7.1 * 10^{10}} = 0.0043661 \quad (5)$$

Germainscher Lloyd (Germanischer Lloyd, 2010) specifies the material safety factors for the wind turbine. The partial safety factors for the ultimate strength design of the blade were derived from the following expression:

$$\gamma_{M_x} = \gamma_{M0} \prod_i C_{ix} \quad (6)$$

Where, γ_{M0}=1.35 for all conditions, C_{ix} = aging (1.35) temperature (1.1), automated layup (1.1), and post-cured laminate (1) dependent factors. It is determined that a material safety factor f_s of 2.205 is required for wind turbine blades. (Hand et al., 2021). Hence, the allowable tensile and compressible strain becomes

$$\epsilon_{t,c\ (allow)} = \frac{0.0043661}{2.205} = 0.00198 \quad (7)$$

The thickness of the blade surface and spars was estimated to achieve the allowable tensile and compressible strain for aluminum material. The deformation and maximum equivalent stress were then compared with homogenized composite material.

2.2 Computational fluid dynamic (CFD) of blade

Two different CFD simulations were carried out to calculate the pressure load on the blade: steady state simulation for extreme loading conditions, and transient simulation for normal operating conditions. In this article, the CFD was used to solve the Navier-Stokes equation of fluid flow for incompressible and isothermal conditions. The Reynolds average Navier-Stokes (RANS) method was applied to introduce the turbulence in N-S equation. The turbulence parameters were solved using the widely used $k-\omega$ SST model(Alaimo et al., 2015; Bangga et al., 2020), introducing turbulent kinetic energy (ϵ) and specific dissipation rate (ω). Including these two terms, the

Kathford Journal of Engineering and Management,
ISSN: 2661-6106.

https://kathford.edu.np/Journal/

VOL. 3 ISSUE 1 JUNE 2023, pp. 149-171

continuity and N-S equations were iteratively solved using pressure based SIMPLE algorithm ("Ansys Fluent Theory Guide," 2013).

2.2.1 Model development

Two different CFD models were developed for steady and transient CFD simulation using a similar meshing strategy. The complex blade geometry was captured using the structured meshing of the blade. In doing so, the blade cross-section was divided into 105 nodes with concentrated nodes at sharp leading and trailing edges. The blade span was divided into 120 divisions. The first cell height was calculated such that the Y^+ value lies in the viscous sublayer (below 5) and the boundary layer flow was properly captured. Assuming a free stream velocity of 80 m/s, the first cell height was estimated at around $5 * 10^{-6}$ m in *https://www.pointwise.com/yplus*. 25 layers of inflation layer is added around the blade wall to create H-type grid with a constant growth rate of 1.2. Likewise, structured meshing of the blade tip was completed with adding 50 inflation layers on the top of the blade. For steady-state simulation, a single fixed domain was created as shown in Figure 2. Details of the fixed domain are presented in Table 3. For transient simulation, the inner rotating domain and the outer fixed domain were created. The shape of the inner rotating domain is the frustum of an inverted cone 82m high with a base radius of 40m and a top radius of 100 m. The outer fixed domain also uses hexahedral mesh and has a C-shaped inlet with a radius of 400 m. Therefore, the width of the fixed domain is 800m. The outer domain is 270m in height and 1400m in length. The center of the inner domain is located 400m from the inlet. The extreme loads on the blade were calculated from the CFD simulation. The inner rotating domain mesh worked out for simulation on moving blade was extended to create mesh this time. By associating these, the model attained a single domain with hexahedral mesh. The meshing around the blade airfoil and tip of the blade are clearly presented in Figure 3.

Kathford Journal of Engineering and Management,
ISSN: 2661-6106.

https://kathford.edu.np/Journal/
VOL. 3 ISSUE 1 JUNE 2023, pp. 149-171

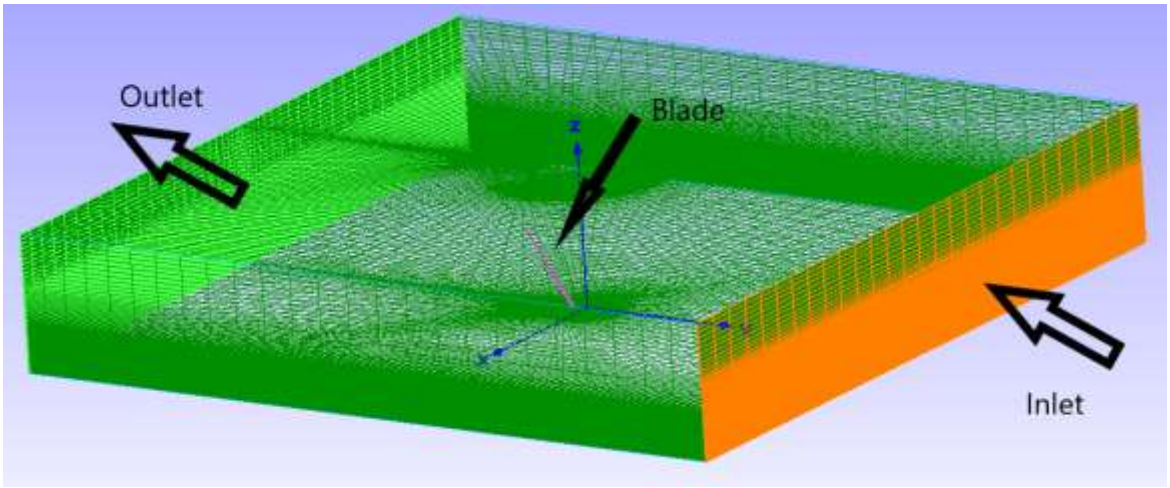

Figure 2. CFD domain for ultimate strength load on blade

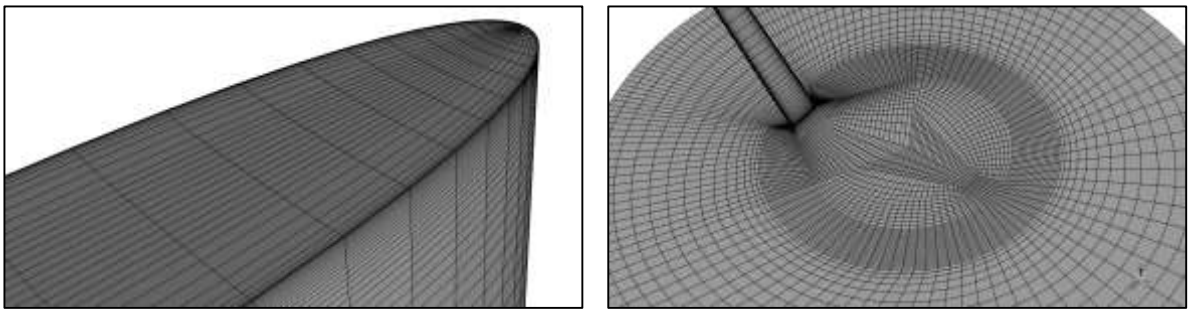

(a) **(B)**

Figure 3. (a) Blade tip meshing (b) Meshing of inner rotating domain

Table 3. Details of the domain for the ultimate strength test

Domain	Dimension
CFD domain for ultimate strength load on the blade	Cuboidal shape: 800*800*140m, Blade: 415m from inlet (2,525,141 cells)

2.2.2 Solution Procedure

Standard properties of air were used for the simulation. The second-order upwind and second-order implicit schemes were used for spatial and temporal discretization respectively, when needed in the CFD simulation. The transport quantities on boundary faces were calculated using the least square cell-based method. Under relaxation was used to improve convergence in the solution. For boundary conditions (BC), the front side and back side of the fixed domain

Kathford Journal of Engineering and Management,
ISSN: 2661-6106.

https://kathford.edu.np/Journal/

VOL. 3 ISSUE 1 JUNE 2023, pp. 149-171

were set to velocity inlet and pressure outlet respectively. The turbulent intensity and viscosity ratio were set to 5% and 10 respectively at inlet and outlet. The other sides were specified as symmetry BC. The blade wall was specified as a zero-shear slip wall. For transient simulation, the inner domain was rotated clockwise at TSR 5 ($TSR = \omega R/V$), as estimated for similar type turbine(Soraghan, 2014). Here, ω is the rotational speed of the turbine, R is the radius of the turbine at the tip and $V = 12\, m/s$ is the designed velocity of the turbine. The blade BC in such case is a moving wall having no relative motion to the inner domain. The time step for transient simulation was set to 0.01938 seconds, which corresponds to a 1-degree movement of the blade(Almohammadi et al., 2013).

For steady-state simulation, the mathematical solution was considered converged for each time step with all the residuals went below 10^{-5}. The coefficient of drag in the direction of inlet velocity was monitored to validate the convergence of the solution. The coefficient of drag was calculated as: $C_d = \frac{2D}{\rho A_1 V_\infty^2}$, where D is the drag force calculated by Fluent, A_1 is the area of the blade projected normal to inlet velocity, calculated to be $258\, m^2$, and ρ is the density of the air. The computation was done until the convergence having airflow around the blade 70 m/s.

For transient simulation, the computational solution was considered converged for each time step when the residual for continuity goes below 10^{-3} and other residuals below 10^{-5} .The

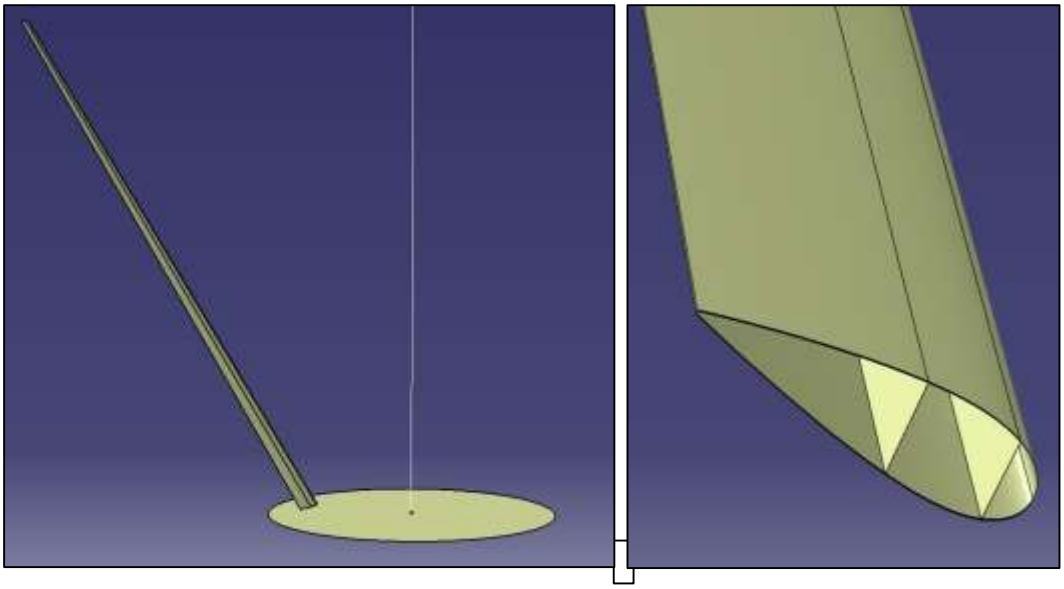

Figure 4. Blade orientation and structural layout in CATIA V5

Kathford Journal of Engineering and Management,
ISSN: 2661-6106.

https://kathford.edu.np/Journal/

VOL. 3 ISSUE 1 JUNE 2023, pp. 149-171

convergence was also monitored by calculating a coefficient of moment (Cm) for each time step, which is calculated as $Cm = \tau / \frac{1}{2} \rho V_\infty^2 AR$. Here, τ is the torque developed on the vertical z-axis by the blade, A is the frontal area of the turbine, and R is the tip radius of the turbine. For reference value, A and R was taken as 6020 m^2 and 66.62m respectively from the dimension of a 2 MW turbine. The performance coefficient of the blade was calculated by $Cp = Cm * \lambda$, where; $\lambda = \omega V_\infty$ is the TSR of the blade.

Using FSI, the pressure load on the blade for steady and transient simulations was transferred to the FEM model of the blade to study structural behavior.

2.3 Blade structure

The blade structure model was created in CATIA V5 using a generative shape design. The model orientation and inside details are shown in Figure 4. Initially, the blade with four shear webs at 20%, 30%, 60%, and 80% of the chord length along the span of the blade was tested for ultimate strength. After performing a mesh independency test on the blade structure with ultimate strength loading condition, the deformations on the blade were studied for the other two models. The other two models were designed by varying the number of shear webs and changing their position on the blade. The two-shear web blade model was made by placing shear webs at 15 % and 50 % of the airfoil chord, taking the reference from the blade structure designed by Hand, Kelly(Hand et al., 2021). The three-shear web blade model was designed with shear webs at 30%, 60%, and 90 % of the airfoil chord for comparison. The geometric model was imported into ANSYS workbench for the finite element analysis.

2.4 Finite Element Analysis (FEA) modeling of the blade

The mathematical model for the FEA modeling of wind turbine blade elements is based on shell theory. Conceptually shell theory is an extension of Euler-Bernoulli's beam theory. Euler-Bernoulli beam theory is a 1D simplification of a beam where the deformations on a 3D beam are calculated by determining how a midline representing the beam takes displacement and rotation(Bauchau & Craig, 2009). Plate theory, a simpler form of shell theory, introduces a 2-D mid-surface instead of the midline. Here, the displacement and rotation of the mid-surface were used to calculate how every point within the beam moves. The objective was then to find out finding the deformed mid surface such that potential energy is minimized. Shell theory takes this idea and generalizes it to the curved surfaces. Local coordinates are needed to define deformations of curved surfaces unlike in plate theory, hence the entire calculation became quite complicated. For numerical solutions, the mathematical model was discretized so

Kathford Journal of Engineering and Management,
ISSN: 2661-6106.

https://kathford.edu.np/Journal/

VOL. 3 ISSUE 1 JUNE 2023, pp. 149-171

that the deformation is defined on a distinct number of nodes rather than the whole surface. The values on any other location on the surface can be determined using values on the node by using the interpolation function. Each node has 6 degrees of freedom for displacement on the X, Y, Z-axis, and rotation about those axes. SHELL181 element used in this article has four nodes for each element defining the motion. SHELL181 is supposed to be favorable for analyzing thin to moderately thick shell structures(ANSYS, 2009).

Initially, FEA was conducted to study mesh independency, comparing different shear web models and, analyzing blade structure. The FEA of the blade was performed in Ansys Static Structural after obtaining pressure load from CFD simulation. The structured meshing of the turbine blade was done using edge sizing and face meshing in ASNYS Mechanical. The number of mesh was varied to test mesh independency for FEA simulation. For boundary conditions, the base of the blade was provided with fixed support. The blade doesn't receive any support anywhere else because the model is towerless. The gravitational load acts from the center of gravity of the blade.

The four-shear web blade model of the blade is then analyzed at eight different azimuthal positions as the blade rotates around the central axis. The purpose of the study is to analyze steady-state deformation and, maximum equivalent stress developed because of wind load and weight of the blade. The blade position was rotated to the required azimuthal position in the Design Modeler. On ASNYS Static Structural, the meshing for the FEA model of the blade is similar to Type D mesh. The pressure loads on the blade were imported to ASNYS Static Structural as done for the ultimate strength test. For eight different azimuthal positions (0°,45°,90°, 135°,180°, 225°,270° and 315°), the pressure load on the blade obtained from the CFD simulation of the blade at TSR 5 was applied to the blade. The azimuthal positions of the blade is shown in the Figure .

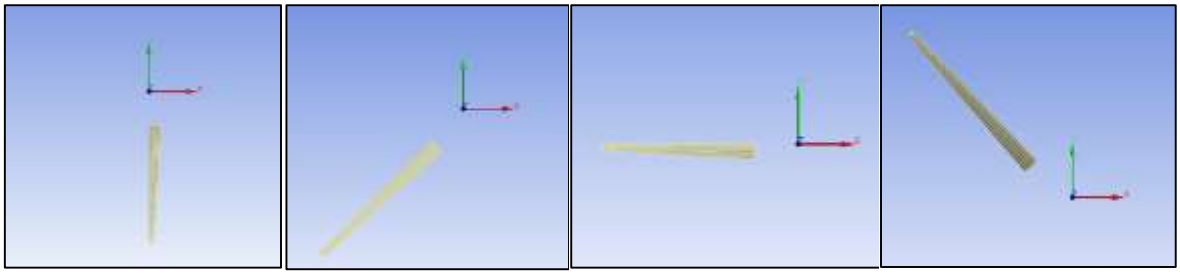

(a) **(b)** **(c)** **(d)**

Kathford Journal of Engineering and Management,
ISSN: 2661-6106.

https://kathford.edu.np/Journal/

VOL. 3 ISSUE 1 JUNE 2023, pp. 149-171

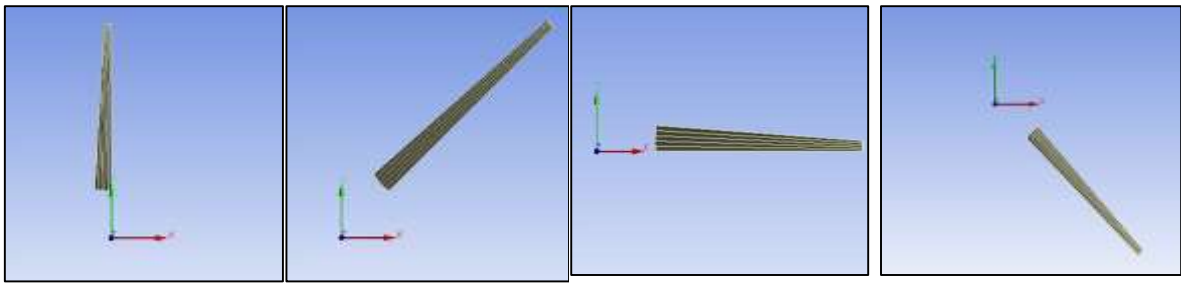

(e) (f) (g) (h)

Figure 5. Blade azimuthal position: (a) 0° ,(b) 45° ,(c) 90°, (d) 135°, (e)180°, (f)225°, (g)270°, and (h)315°

3. RESULTS AND DISCUSSION

3.1. CFD simulation results

The steady-state CFD simulation to obtain aerodynamic load at extreme conditions (70 m/s) is found to converge after obtaining a consistent drag coefficient of 1.03 and residual below the set criteria. The development of the flow is checked using a visual representation of pressure on the blade surface and, velocity contour around the blade airfoil at 60m height from the base as shown in Figure 6. The obtained load from free stream air is later used to perform FSI and calculate deformation, equivalent stress, and equivalent strain concentration.

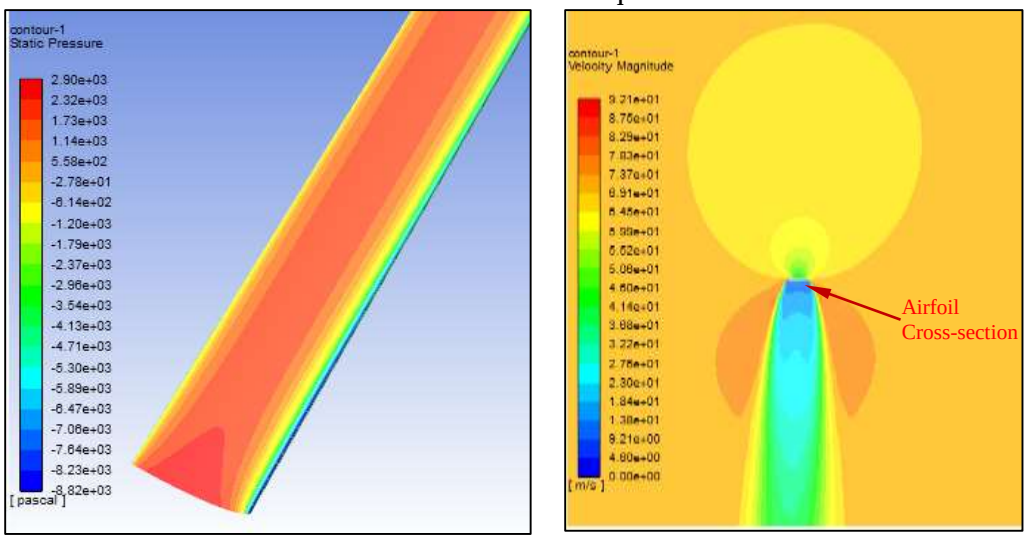

(a) (b)

Figure 6. (a) Static pressure on the blade at 70 m/s (b) velocity contour on XY plane at 60m height

Kathford Journal of Engineering and Management,
ISSN: 2661-6106.

https://kathford.edu.np/Journal/

VOL. 3 ISSUE 1 JUNE 2023, pp. 149-171

The convergence of transient simulation is verified after obtaining residual below the set criteria and the periodic moment coefficient of the blade after 5^{th} rotation as shown in Figure 7(a). The rotation is allowed to fully develop flow around the blade. The average Cp developed by the blade is calculated as 0.1749. The Cp of the blade as it rotates clockwise from 0° azimuth position to 360°azimuth position is shown in Figure 7(b). The aerodynamic loads acting on blades at 8 different azimuth positions are later used to conduct one-way FSI and estimate the deformation and maximum equivalent stress of the blade at those azimuth positions.

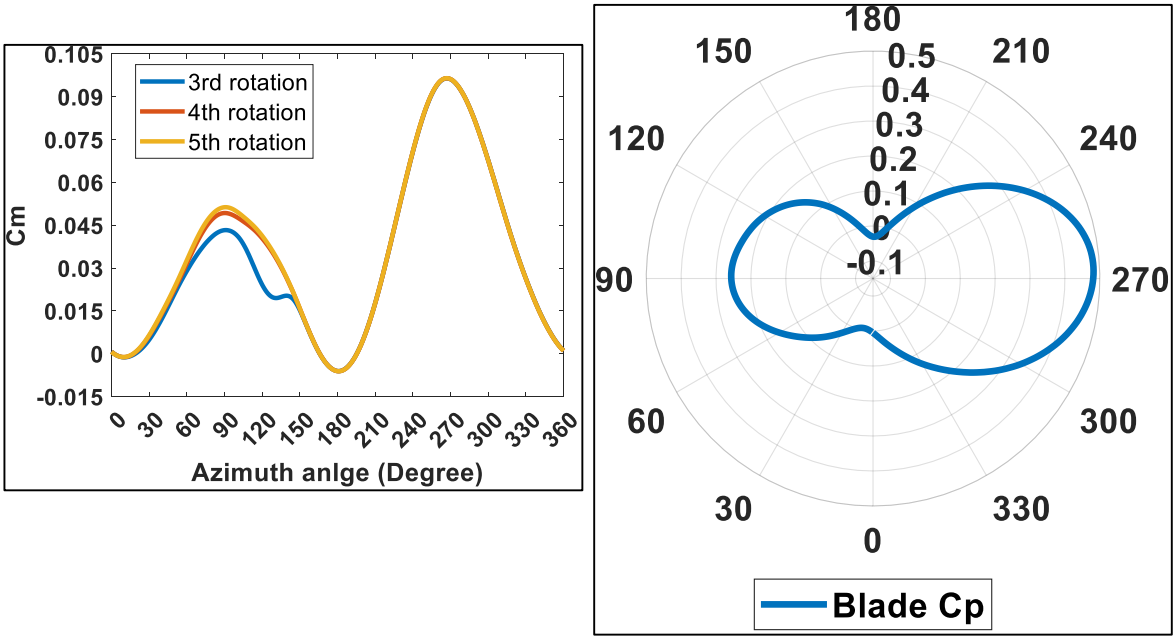

(a) **(b)**

Figure 7. (a)Azimuth angle Vs Cm curve with increasing rotation of blade (b) Polar plot of Cp at all azimuth positions of the blade

3.2 FEM simulation results

The pressure load developed on the blade after CFD simulation is matched to the FEA blade model in Static Structural. The exact matching is confirmed through visual inspection as shown in Figure

.

Kathford Journal of Engineering and Management,
ISSN: 2661-6106.

https://kathford.edu.np/Journal/
VOL. 3 ISSUE 1 JUNE 2023, pp. 149-171

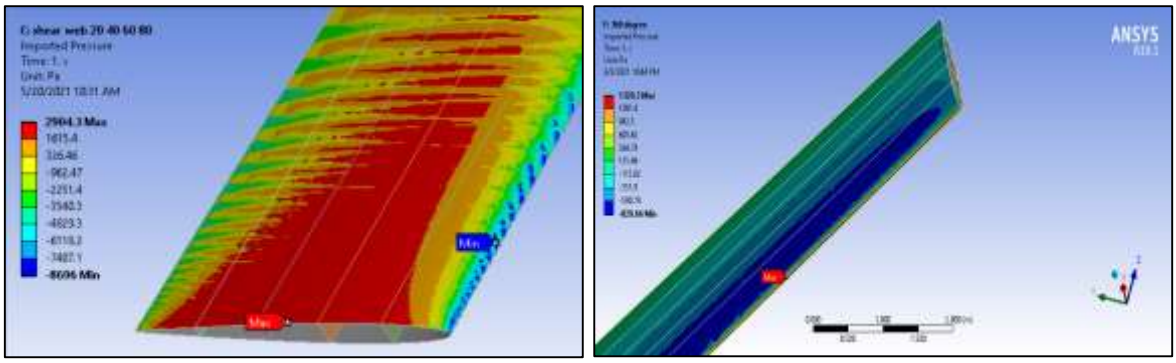

(a) **(b)**

Figure 8. Mapping of pressure load on the blade (a) Ultimate strength test (b)0° azimuth position at TSR 5

3.2.1 Mesh independency test

The maximum deformation at the tip of the blade and maximum equivalent stresses on the blade are studied for different mesh densities to obtain a mesh-independent solution. The number of elements is varied by changing the number of nodes on the edges of the blade. Initially, only pressure loads are applied on the blade for the mesh independency test. The blade with four shear web models is selected for performing the simulation. The thickness for each section of the blade is set to be 0.1m. Material properties of aluminum alloy are selected for the simulation. The independency is checked for maximum deformation and maximum equivalent stress.

Table 4. Details of the number of elements and respective deformation and stress

Mesh	Max. total deformation (m)	Max. equivalent stress (Pa)	Element
Type A	6.6536	6.2865E7	7,437
Type B	6.4273	8.5647E7	67,000
Type C	6.4088	8.5546E7	117,000
Type D	6.384	1.346E8	422,411
Type E	6.3876	1.4368 E8	565,235
Type F	6.386	1.4487 E8	613,211

Table 4, it can be seen that the independency of results for total deformation is achieved quickly. While the equivalent stress calculation depends on grid resolution even for a finer mesh. The mesh distribution and maximum

Kathford Journal of Engineering and Management,
ISSN: 2661-6106.

https://kathford.edu.np/Journal/

VOL. 3 ISSUE 1 JUNE 2023, pp. 149-171

equivalent stress of Type A and Type E mesh is shown in Figure . Type E mesh is selected for further calculation such that mesh-independent solution is achieved with reasonable computational cost. The blade cross-section is divided into 160 nodes. The blade is divided into 2600 nodes along the span and 10 nodes are allotted for each shear webs on cross-section.

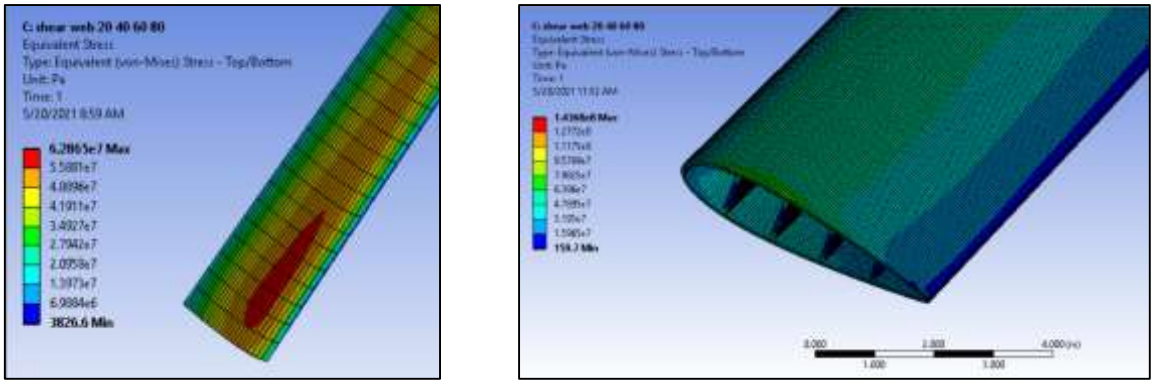

(a) **(b)**

Figure 9. Stress distribution on (a) Type A mesh (c) Type E mesh

3.2.2 Comparison of two, three, and four shear web blade model

The maximum deformation of the blade is compared for three blade models. The loading condition is similar to the mesh independency test. The value of total deformation at the tip of the blade and the location of shear webs for two, three, and four shear web blade models are shown in Figure 10(a), 10(b) and 10(c) respectively. The lowest deformation of 6.382 m is obtained for the four-shear web model. The difference in deformation for all three models is within 0.4 m, thus not showing considerable changes in deformation by increasing the number of shear webs. However, four shear web model is chosen for further analysis as it is supposed to have better structural stability under other operating conditions. On the three-shear web model, the shear web is placed at 90% of the chord. This is located near the trailing edge. From the comparison of two and three shear web models, it is concluded that the shear web near to trailing edge doesn't provide significant structural support.

Kathford Journal of Engineering and Management,
ISSN: 2661-6106.

https://kathford.edu.np/Journal/

VOL. 3 ISSUE 1 JUNE 2023, pp. 149-171

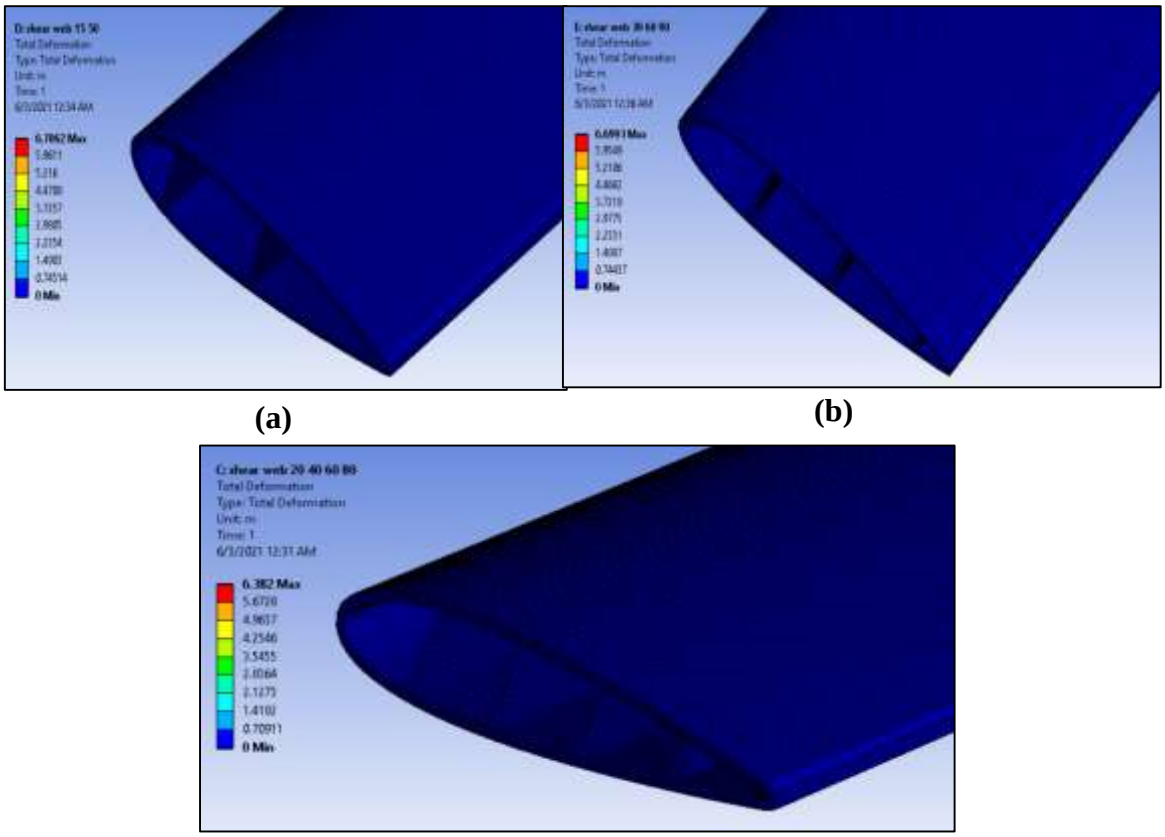

Figure 10. Blade structure and deformation (a) Two shear web (b) Three shear web (c) Four shear web

3.2.3 Analysis of blade structure

Previously, aerodynamics load is applied to the blade for mesh independency test and analyzing the effect of the variable shear web on blade structure. Adding gravitational load, the maximum deformation, maximum equivalent strain and maximum equivalent stress on the blade increases. The ultimate strength test of the blade is performed changing its thickness to pass the allowable strain limit. A constant 0.1m thick blade, used previously, shows a deflection of 29.583m on adding gravitational load. Therefore, the thickness of the blade is varied to reduce deflection and to limit equivalent strain to less than the maximum allowable strain. The simulation results from varying thicknesses of blade surface and shear webs are listed in Table 5. The first three models have a constant thickness-shear web of 0.05m. Under steady-state loading for the ultimate strength test, the allowable elastic equivalent strain is obtained for the last two models. These two models are also studied using

Kathford Journal of Engineering and Management,
ISSN: 2661-6106.

https://kathford.edu.np/Journal/

VOL. 3 ISSUE 1 JUNE 2023, pp. 149-171

homogenized material properties of composite material for wind turbine blades. The simulation results for total deformation, maximum equivalent stress, and maximum equivalent strain are presented in Table 6. The result showed that the behavior of wind turbine blades can be significantly improved using composite materials. There will be less deformation on the blade and the weight of the blade decreases considerably. Further analysis of blade structure is performed with the blade model having a tapered blade surface thickness of 0.3 at the base to 0.01 at the tip and a shear web with a thickness of 0.05m at the base to 0.01m at the tip.

Table 5. Total deformation, maximum strain, and blade weight for different thicknesses of blade for aluminum material

SN	Blade thickness from base to tip (m)	Shear web thickness from base to tip(m)	Total deformation (m)	Max. Equivalent elastic strain (allowable 0.00198)	Blade weight (tonne)
1	0.1 (Constant)	0.1(Constant)	29.583	0.009697	209.82
2	0.3 to 0.05	0.05(Constant)	9.3504	0.0028484	404.41
3	0.2 to 0.01	0.05(Constant)	12.494	0.00326	248.6
4	0.3 to 0.01	0.05 (Constant)	8.4096	0.0024437	368.4
5	0.3 to 0.01	0.05 to 0.01	8.2509	0.001652	327.55
6	0.25 to 0.01	0.05 to 0.01	10.059	0.0018926	276.94

1 tonne=1000 kg

Table 6. Total deformation, maximum strain, and blade weight for different thicknesses of blade for homogenized material

SN	Blade thickness from base to tip (m)	Shear web thickness from base to tip(m)	Total deformation (m)	Max. Equivalent elastic strain	Blade weight (tonne)
1	0.3 to 0.01	0.05 to 0.01	3.5539	0.0013168	183.29
2	0.25 to 0.01	0.05 to 0.01	4.4074	0.0016985	154.96

Kathford Journal of Engineering and Management,
ISSN: 2661-6106.

https://kathford.edu.np/Journal/
VOL. 3 ISSUE 1 JUNE 2023, pp. 149-171

3.2.4 Analysis of deformation and maximum stress of the blade at different azimuth positions

From the observation, the critical area where maximum equivalent stress would be generated is found to be on the base of the blade. The critical stress developed at the base at 0° azimuthal position is shown in Figure 11. The periodic nature of maximum equivalent stress concentration is also observed as shown in Figure . Evidently, the maximum and minimum stress concentration occurs when the blade is perpendicular to the direction of the airflow. The maximum deformation of the blade tip and highest equivalent stress concentration is obtained at 90° azimuth as observed in Table 7. The deflection for an aluminum alloy blade is 7.4m which is 138% more than the 3.1m deflection calculated for the homogenized composite blade. Similarly, the minimum deformation of the blade tip and lowest equivalent stress concentration is obtained at 270° azimuth. The minimum deflection for aluminum alloy is 3m which is 604% more than 0.43m deflection for homogenized composite blade. The structural strength of composite blade is again proved to be superior to Aluminum blade while testing at normal operating conditions.

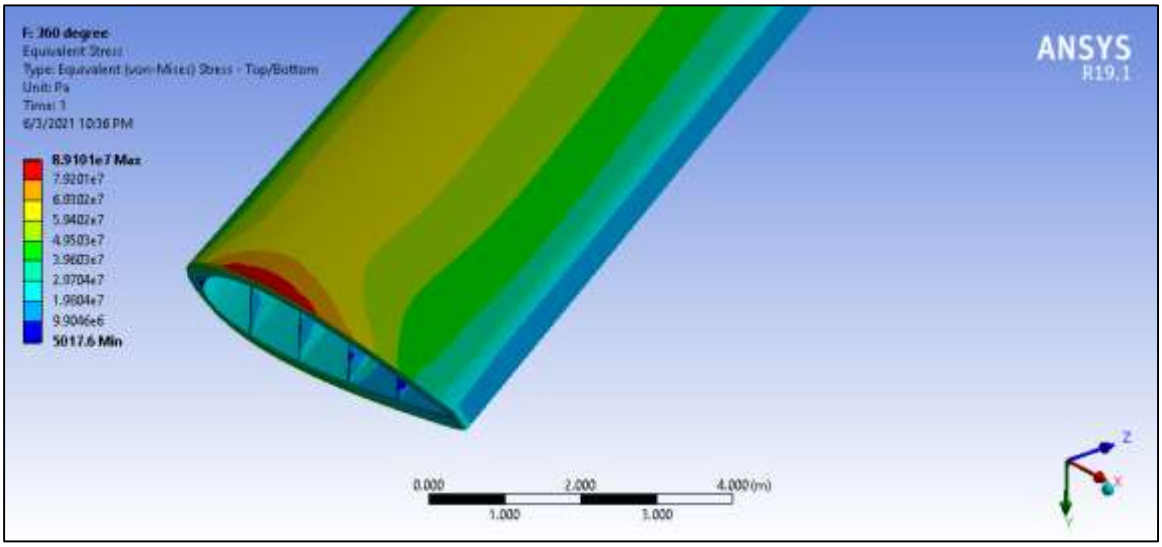

Figure 11. Stress on the blade due to pressure and gravitational load at azimuthal position 0°

Kathford Journal of Engineering and Management,
ISSN: 2661-6106.

https://kathford.edu.np/Journal/
VOL. 3 ISSUE 1 JUNE 2023, pp. 149-171

Table 7. Max. deformation, stress, and strain details for the different azimuthal position

	Max. Deformation (Al-alloy) (m)	Max. Equivalent Stress (Al-alloy) (Pa)	Max. Equivalent Strain (Al-alloy)	Max. Deformation homogenized composite (m)
45 degree	6.4379	9.7804E7	0.0013775	2.5185
90 degree	7.3564	1.0442E8	0.0014707	3.103
135 degree	7.0639	1.0261E8	0.0014453	2.9168
180 degree	5.3238	8.9815E7	0.001265	1.8104
225 degree	3.4539	7.5876E7	0.0010687	0.6935
270 degree	3.0365	7.3438E7	0.0010343	0.43508
315 degree	3.9261	8.0274E7	0.0011306	0.93425
360 or 0 degree	5.2092	8.9101E7	0.0012549	1.7372

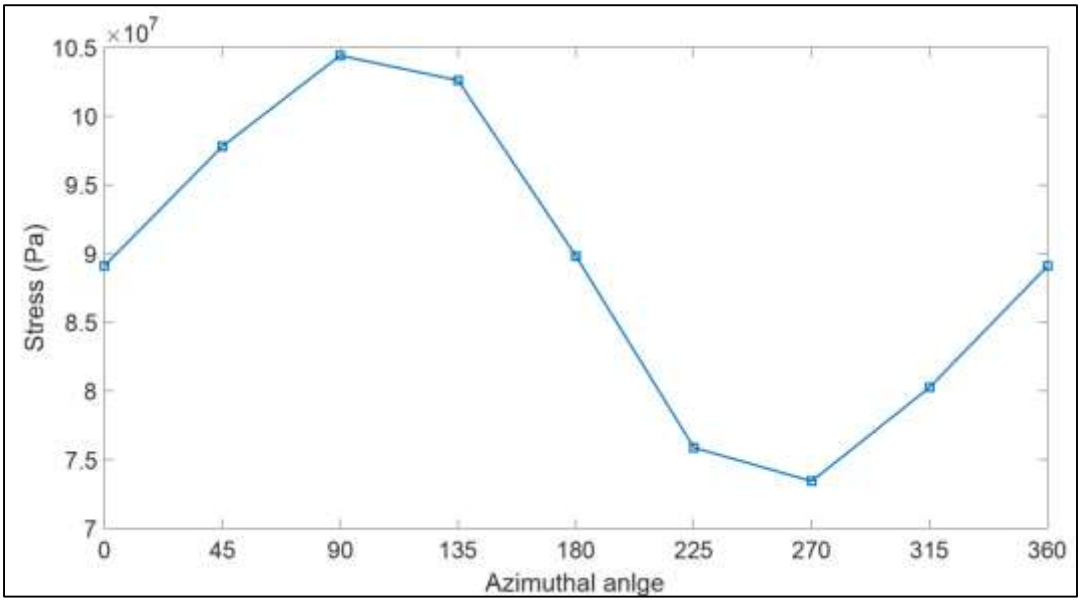

Figure 12. Variation of maximum stress on the blade with azimuthal angle

4. CONCLUSIONS

The study of the tower-less V-shaped VAWT blade structure under aerodynamic load and gravity compliments the research towards the application of large-scale VAWT in offshore areas. The findings of the research provide an intuitive idea of the selection of material and the requirement of additional supports for the turbine.

Kathford Journal of Engineering and Management,
ISSN: 2661-6106.

https://kathford.edu.np/Journal/

VOL. 3 ISSUE 1 JUNE 2023, pp. 149-171

In this paper, a conceptual design of the V-VAWT blade structure was proposed and the structural behavior of the blade was studied at different loading conditions. The purpose of the study was to analyze the feasibility of towerless turbine blades for V-VAWT by applying different material properties to the blade. The blade was used for 2 MW V-VAWT and it was 90m long inclined at 35° to the vertical axis and tapered with a base chord length of 5m and tip chord length of 2m. The thickness of the blade surface and shear webs were varied to select a feasible blade structure after performing an ultimate strength test using aluminum alloy properties for the blade. Moreover, the comparison of aluminum alloy blades with composite material blades was performed. The proposed blade model was then studied for maximum deflection of the blade tip, maximum equivalent stress, and maximum equivalent strain under its own weight and aerodynamic load at TSR 5 for eight different azimuthal positions of the turbine.

Initially, the aerodynamic load on the blade was calculated using steady-state RANS CFD simulation in ANSYS fluent. The pressure load on the blade was obtained after the residual was converged to the specified limit and the consistent drag coefficient of 1.03 was achieved. The load was transferred by one-way FSI to the FEM model of the blade. It was used to study mesh independency of 6 different FEM blade models, and to analyze the effect of shear webs in the deformation of the blade. The 4-shear web model of the blade with the Type E mesh model was then used for the ultimate strength test of the blade. The blade was tested using extreme loading conditions according to IEC standards. In doing so, the maximum pressure load on the blade because of $70\ m/s$ wind velocity and the weight of the blade acting from the center of gravity was applied in ANSYS static structural software. The thickness of the blade surface and shear webs were varied for aluminum alloy blades to test for maximum allowable strain criteria. The blade model having tapered blade surface thickness with 0.3m at the base to 0.01 m at the tip of the blade and tapered shear web thickness of 0.05m at the base and 0.01m at the tip of the blade was selected from the ultimate strength test. The blade model has the lowest deformation of 8.25m and a Maximum Equivalent Strain of 0.0016. The aluminum alloy blade was compared with a homogenized composite material blade under similar loading conditions. The maximum deformation at the blade tip was obtained to be $3.55m$ which is 138% less than that for the aluminum alloy blade. The total weight of the composite blade is calculated to be 183.29 tonne whereas the aluminum blade has 327.55 tonne weight. From this observation, the lighter-weight composite material blade is suggested for the V-VAWT blade.

The other study included the transient CFD simulation to calculate the aerodynamic load on the blade at different azimuthal positions. The CFD simulation converged after 5 complete rotations of the

blade. The pressure load on the blade for eight different positions of the blade was applied using a similar approach as in the previous case. The periodic maximum deflection of the blade tip, maximum equivalent stress, and maximum equivalent strain of the blade were observed for both aluminum and composite blades after performing the simulation for eight different azimuthal positions. The periodicity for maximum equivalent stress was also plotted. The maximum deformation for homogenized composite blades was found to be less than that for the aluminum alloy blades in all cases, suggesting its better performance. From both case studies in the paper, it was found that deflection at the tip of the blade is still more than half a meter while using both materials; aluminum alloy and composite material. This scale of deflection is not allowed for turbine blades. An additional support is hence required for the blade structure to reduce deflection. Mooring the tip of the blade with ropes could be an alternative solution to reduce the deflection.

5. FUTURE WORKS

The following are the recommendations for the future works:

1. The next step will be studying V-VAWT structure by applying the inertial load and the additional support to the blade.
2. The mesh independency of CFD simulation is to be performed to reduce error in the simulation.
3. The real properties of composite material can be produced using Ansys Pre composite instead of using homogenized material properties. In this way, we can add composite layers of uniaxial and biaxial composites to develop orthotropic nature of blade material.
4. The base of the blade is to be modeled which could reduce maximum equivalent stress and maximum equivalent strain of the blade, thus improving structural robustness.

6. REFERENCES

1. Alaimo, A., Esposito, A., Messineo, A., Orlando, C., & Tumino, D. (2015). 3D CFD analysis of a vertical axis wind turbine. *Energies*, *8*(4), 3013–3033.

2. Almohammadi, K. M., Ingham, D. B., Ma, L., & Pourkashan, M. (2013). Computational fluid dynamics (CFD) mesh independency techniques for a straight blade vertical axis wind turbine. *Energy*, *58*, 483–493.

3. ANSYS. (2009). Structural Analysis Guide Release 12.0. In *ANSYS, Inc.*

4. Ansys Fluent Theory Guide. (2013). In *ANSYS Inc., USA* (Issue November).

5. Bangga, G., Dessoky, A., Wu, Z., Rogowski, K., & Hansen, M. O. L. (2020). Accuracy and consistency of CFD and engineering models for simulating vertical axis wind turbine loads. *Energy*, *206*, 118087.

6. Barnes, R. H., & Morozov, E. V. (2016). Structural optimisation of composite wind turbine blade structures with variations of internal geometry

configuration. *Composite Structures*, *152*, 158–167.

7. Bauchau, O. A., & Craig, J. I. (2009). *Euler-Bernoulli beam theory BT - Structural Analysis* (O. A. Bauchau & J. I. Craig (Eds.); pp. 173–221). Springer Netherlands.

8. Brøndsted, P., Lilholt, H., & Lystrup, A. (2005). Composite materials for wind power turbine blades. *Annual Review of Materials Research*, *35*(1), 505–538.

9. Commision, I. E. (2014). *IEC 61400-1 Wind turbine generator systems - Part 1: safety Requirements*.

10. David, P., & Julia, C. (n.d.). Novel offshore vertical axis wind turbines. *Cranfield University*.

11. Germanischer Lloyd. (2010). *Regulation of the certification of wind energy conversion systems, rules and regulations IV: non marine technology Part 1*.

12. Griffith, D. T., Barone, M., Paquette, J., Owens, B., Bull, D., Simao-Ferriera, C., & Goupee, A. (2018). Design Studies for Deep-Water Floating Offshore Vertical Axis Wind Turbines. In *U.S. Department of Energy* (Issue June).

13. Hand, B., Kelly, G., & Cashman, A. (2021). Structural analysis of an offshore vertical axis wind turbine composite blade experiencing an extreme wind load. *Marine Structures*, *75*(June 2020), 102858.

14. Lin, J., Xu, Y. lin, & Xia, Y. (2019). Structural analysis of large-scale vertical axis wind turbines Part II: Fatigue and ultimate strength analyses. *Energies*, *12*(13).

15. Owens, B. C., & Griffith, D. T. (2014). Aeroelastic stability investigations for large-scale vertical axis wind turbines. *Journal of Physics: Conference Series*, *524*(1).

16. Soraghan, C. E. (2014). Aerodynamic Modelling and Control of Vertical Axis Wind Turbines. In *Ph.D Thesis*.

17. Sutherland, H. J., Berg, D. E., & Ashwill, T. D. (2012). A Retrospective of VAWT Technology. *Security*, *January*, 1–64.

18. Tangler, J. L. (2000). *The Evolution of Rotor and Blade Design* (Issue July).

19. Tarfaoui, M., Nachtane, M., & Boudounit, H. (2020). Finite Element Analysis of Composite Offshore Wind Turbine Blades under Operating Conditions. *Journal of Thermal Science and Engineering Applications*, *12*(1).

20. Tjiu, W., Marnoto, T., Mat, S., & Ha, M. (2015). Darrieus vertical axis wind turbine for power generation II : Challenges in HAWT and the opportunity of multi-megawatt Darrieus VAWT development. *Renewable Energy*, *75*, 560–571.

21. Tjiu, W., Marnoto, T., Mat, S., Ruslan, M. H., & Sopian, K. (2015). Darrieus vertical axis wind turbine for power generation I: Assessment of Darrieus VAWT configurations. *Renewable Energy*, *75*, 50–67.

22. Ullah, H., Ullah, B., & Silberschmidt, V. V. (2020). Structural integrity analysis and damage assessment of a long composite wind turbine blade

under extreme loading. *Composite Structures*, *246*(December 2019), 112426.

23. Wang, L., Kolios, A., Nishino, T., Delafin, P. L., & Bird, T. (2016). Structural optimisation of vertical-axis wind turbine composite blades based on finite element analysis and genetic algorithm. *Composite Structures*, *153*(January 2015), 123–138.